ELECTROCHEMICAL CHARACTERISTICS OF AN INTERDIGITATED MICROBAND ELECTRODE ARRAY OF BORON-DOPED DIAMOND FILM

Wei ZHANG[a1,b,*], Shaoai XIE[a2], Mei LI[a3], Hongjin CHEN[a4], Li MA[a5] and Jinping JIA[b1,*]

[a] *School of Chemistry and Chemical Technology, Shanghai Jiao Tong University, 800 Dongchuan Road, Shanghai, 200240, P. R. China; e-mail: [1] weizhang@sjtu.edu.cn, [2] xie-shaoai@163.com, [3] meili@sjtu.edu.cn, [4] chenhj@sjtu.edu.cn, [5] mali@sjtu.edu.cn*

[b] *School of Environmental Science and Engineering, Shanghai Jiao Tong University, 800 Dongchuan Road, Shanghai, 200240, P. R. China; e-mail: [1] jinpingjia@126.com*

Received July 12, 2008
Accepted October 2, 2008
Published online February 24, 2009

An microband electrode array (MBEA) of a boron-doped diamond (BDD) film was prepared by using the hot-filament chemical vapor deposition (HF-CVD) technique and microfabrication process with a standard photolithography technique. Electrochemical properties of a single MBEA (S-MBEA) and interdigitated MBEA (I-MBEA) of BDD film were studied by cyclic voltammetry (CV) analysis. Charge transfer characteristics were examined by electrochemical impedance spectra (EIS) analysis. A ferri–ferrocyanide redox system was chosen to act as the probe of one-electron transfer processes. The redox reaction was controlled by linear diffusion-limited transport at S-MBEA and quasi-steady-state non-linear diffusion at I-MBEA. A relation between current limit at I-MBEA and sweep rate was obtained with a correlation coefficient greater than 0.93. Hemispherical diffusion was primary at I-MBEA of BDD surface. There were two time constants for the S-MBEA and one time constant for the I-MBEA in the redox system.

Keywords: Boron-doped diamond electrodes; Interdigitated microband electrode array; Charge transfer characteristics; Cyclic voltammetry analysis; Electrochemical impedance spectra; Electrochemistry.

It is well known that the electrochemical response of an electrode is strongly dependent on its geometry, surface structure and substrate material. It has also been noticed that an electrode will exhibit different electrochemical behavior when its size decreased to less than 50 μm in at least one critical dimension[1]. Researchers define an electrode having at least one dimension in the range 10–50 μm as microelectrode (ME) and an electrode with at least one critical dimension below 10 μm as ultramicroelectrode (UME).

doi:10.1135/cccc2008161

Due to a special small geometry of ME, it has a low background charging, small ohmic drop, small current, high current density and small time constant. All these advantageous properties attract researchers to investigate how to employ it in analytical chemistry and physiological fields. But the undesirable small current would restrict the scope of electrochemical detection. It can be overcome by using an array of individual microelectrodes (MEA) in which each ME is insulated from the other by dielectric materials such as silicon nitride or silicon dioxide. MEA can improve the Faraday current by increasing the active electrode area retaining all advantages of ME. An ordered MEA with appropriate interelement space can improve signal-to-noise (S/N) ratio and sensitivity, reduce limits of detection and make use of smaller sample volume[2,3].

In addition, as a new electrode material, the boron-doped diamond (BDD) electrode has been disclosed to possess many attractive electrochemical characteristics such as a wide working potential window, very low and stable background current, stable electrochemical response and high resistance to deactivation[4–6]. Planar BDD electrodes have been reported as an amperometric detector for determination of some metal ions[7,8], organic compounds[9,10], drugs[11,12] and pollutants[13] in quantitative electrochemical analysis. Therefore, planar BDD electrodes are considered as promising in microlithographic fabrication of MEA.

The common geometry of MEA is the microdisc electrodes array (MDEA) where the electrodes are arranged in a hexagonal, a square lattice or even in a random manner. Compton et al.[14] found the electrochemical characteristics and proposed theories of regular and random arrays of microdisc electrodes by CV analysis. The disc radius, centre-to-centre separation, diffusion coefficient of the redox species and sweep rate used in CV analysis were the four parameters which could highly influence the slope of CV curves. Girault and co-workers[15] investigated the simulated CV response of a regular microdisc electrode array. The avoidance of diffusional shielding of microdisc arrays was clearly necessary but not sufficient. Other research groups[16,17] proposed electrochemical oxygen transfer reactions and the measurement of sulfate and peroxodisulfate using the MEA of BDD electrodes.

Another common geometry of MEA is the parallel microband electrode array (MBEA)[18–22]. The parallel microbands can also be arranged as interdigitated form in which every group of parallel microbands are alternatively polarized as cathodes or anodes. Nyholm's research group[18] revealed the influence of convection on the degree of redox cycling in interdigitated MBEA (I-MBEA) in a flow system. The conversion and collection efficiencies

could be increased by decreasing the flow rates and by increasing the width of the bands. Kang and co-workers[19,20] discovered that the MBEA of BDD electrodes confirmed theoretical results at slow sweep rates while deviation at high sweep rates were attributed to linear diffusion-limited transport. Katsuyoshi and coworkers[21,22] detected catecholamines by using a microfluidic device integrated with an enzyme-modified pre-reactor for interferent elimination and an interdigitated electrode array.

To obtain a deeper understanding about electrochemical properties and charge transfer characteristics of I-MBEA of BDD film, we measured the $Fe(CN)_6^{3-/4-}$ redox system by CV and electrochemical impedance spectra (EIS) methods.

EXPERIMENTAL

The fabrication processes for the I-MBEA of BDD employed in our work included the following four steps: first, a 5.0 μm-thick diamond thin film was thermally deposited on a silicon (100) substrate by using the hot-filament chemical vapor deposition (HF-CVD) technique at 2500 °C (filament temperature) under H_2 atmosphere containing 2.0% acetone (30 Torr). Next, a 1.0 μm-thick Si_3N_4 layer was grown on the diamond film and then aluminum was sputtered on the Si_3N_4 layer. After a standard photolithography and microfabrication process, the Al layer was eliminated by a solution of H_2SO_4 and H_2O_2. Subsequently, a ca. 1.0 μm-thick BDD thin film was grown on the diamond film by the HF-CVD technique in which acetone was employed as the carbon source, hydrogen as the carrier gas and B_2O_3 as the boron source. The resistivity of BDD film is ca. 6.0×10^{-3} Ω cm. Last, the Si_3N_4 layer was removed with hydrofluoric acid and I-MBEA of BDD was washed with deionized water.

A copper wire was soldered onto the edge of I-MBEA electrode using electric gum water and the epoxy resin was used to fix the electrode surface to obtain an electrode active area of ca. 75.6 mm^2. Prior to electrochemical studies, the as-prepared I-MBEA of BDD electrode was ultrasonically cleaned successively in acetone and ethanol, and then rinsed with deionized water.

Surface morphology of I-MBEA was observed with a scanning electron microscope (SEM, S-2150, Hitachi, Japan). The electrochemical measurements were performed in a three-electrode system by two forms at 298 ± 1 K. First, one group of parallel microbands of the I-MBEA which called single MBEA was used as working electrode and a platinum wire as the counter electrode with a saturated calomel electrode (SCE) as reference electrode. This form is denoted as S-MBEA. Second, two groups of parallel microbands of I-MBEA were used as working electrode and counter electrode with a SCE as reference electrode. Similarly, this form is denoted as I-MBEA. CV curves and impedance plots were recorded using an electrochemical workstation (CHI 660C, Shanghai ChenHua Instrument Company, China). In impedance measurements, the frequency range of 100 kHz to 1 Hz and the modulation amplitude of 5 mV were employed. Static duration was 2 s and open-circuit potential set as initial potential. Impedance spectra were fitted to equivalent circuits by using ZSimpWin software. Before electrochemical analysis, the S-MBEAs of BDD was pretreated by anodic oxidation at +2.5 V (vs SCE) for 40 min to obtain a hydrophilic C–O BDD surface.

Solutions were prepared with deionized water, reagents including $K_4Fe(CN)_6$, KNO_3, H_2O_2, HF and H_2SO_4 solutions (A.R. purity) were supplied by Shanghai Chemical Reagent Limit Company.

RESULTS AND DISCUSSION

Film Characterization

Figure 1 shows SEM photographs of I-MBEA of BDD in different magnification. The image of the BDD film exhibited polycrystalline surface, mainly consisting of triangle facets with micron-size crystallites. The width of microbands, *w*, is 15 μm and the separation between the microbands, *d*, is 75 μm. There are 720 pairs of BDD microbands on the I-MBEA with the active working area ca. 75.6 mm^2. In addition, basing on the relationship between the resistivity of BDD film and the volume percentage of doped boron[23], we conclude that the doping level (the ratio of boron to diamond, B/C) in our work is ca. 2.80×10^3 ppm. The BDD electrode in our work is a moderately boron-doped film.

Electrochemical Characteristics

CV analysis is a widely used technique for characterization of MEA which can estimate the working potential window, the reversibility/irreversibility of electrochemical reaction at the MEA surface and some kinetic parameters. To compare the electrochemical response behavior of I-MBEA and S-MBEA of BDD, we figure out CV curves at the MBEAs of BDD.

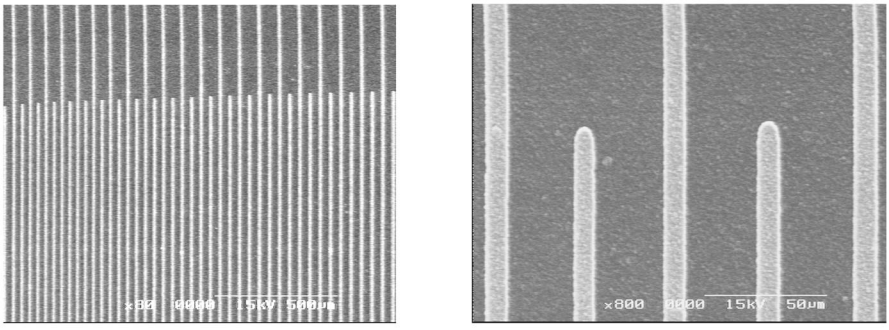

a b

FIG. 1
SEM of the I-MBEA at BDD. a Part of the I-MBEA at BDD, magnification × 80; b part of the I-MBEA at BDD, magnification × 800

Figure 2 illustrates that the working potential windows of S-MBEAs of BDD are similar, S_1-MBEA using one group of parallel microbands of I-MBEA and S_2-MBEA using another group. The working potential windows are in the range from –1.24 to +1.71 V (vs SCE). They exhibit low background charging and a high current density at all S-MBEAs surface.

Electrochemical activities of S-MBEA and I-MBEA of BDD electrodes were examined in 0.1 M $K_4Fe(CN)_6$ and 0.4 M KNO_3 aqueous solutions, respectively (Fig. 3).

In Figs 3a and 3b, CV curves show that the peak potential, E_p (both anodic and cathodic reaction) shifts to negative or positive potential values with increasing sweep rate, v, at S-MBEAs. The peak current, i_p (both anodic and cathodic reaction), increases with increasing v and is directly proportional to the square-root of v (see inset graphs in Figs 3a and 3b). The relationships between i_p and $v^{1/2}$ have been obtained as

$$i_p = 8.58 \times 10^{-4} + 6.31 \times 10^{-3} \sqrt{v} \quad \text{(for } S_1\text{-MBEA)} \tag{1}$$

$$i_p = 8.83 \times 10^{-4} + 5.47 \times 10^{-3} \sqrt{v} \quad \text{(for } S_2\text{-MBEA)} \tag{2}$$

with a standard deviation of the fit lower than 9.21×10^{-5} for S_1-MBEA (R = 0.992) and 6.17×10^{-5} (R = 0.995) for S_2-MBEA. Those predict the redox re-

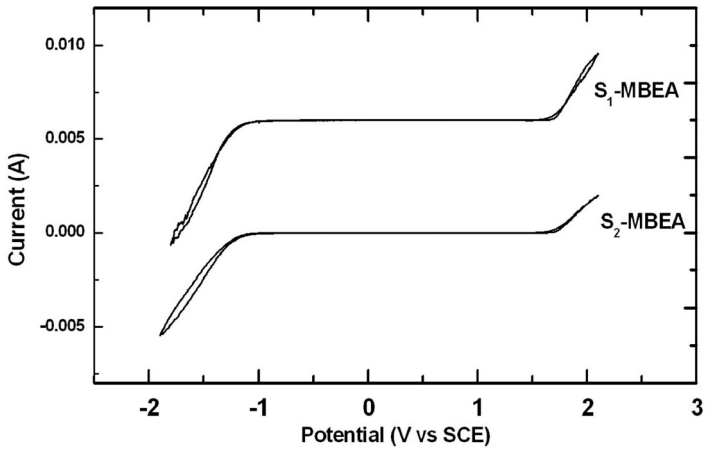

FIG. 2
Cyclic voltammetric curves of S-MBEAs at BDD in 0.1 M H_2SO_4 solution; sweep rate 0.1 V s^{-1}

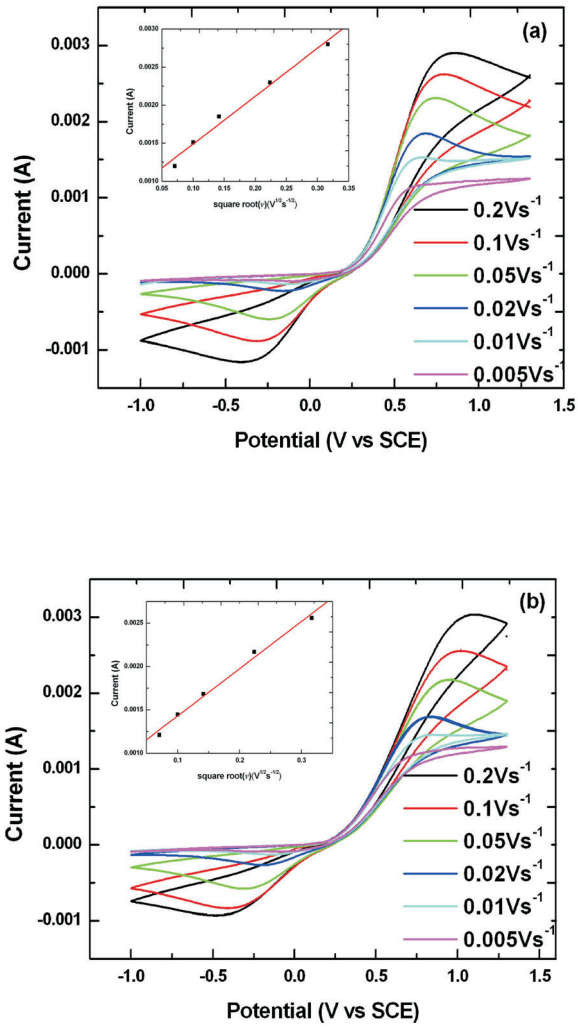

FIG. 3

Cyclic voltammetric curves of S-MBEAs and I-MBEA at BDD in 0.1 M $K_4Fe(CN)_6$ and 0.4 M KNO_3 solution at different sweep rates. a S_1-MBEA at 0.2, 0.1, 0.05, 0.02, 0.01 and 0.005 V s^{-1}; inset graph: linear fit for i_p and square-root of v. b S_2-MBEA at 0.2, 0.1, 0.05, 0.02, 0.01 and 0.005 V s^{-1}; inset graph: linear fit for i_p and square-root of v. *c* I-MBEA at different v: 0.005 (*1*), 0.01 (*2*), 0.02 (*3*), 0.03 (*4*), 0.04 (*5*) and 0.05 (*6*) V s^{-1}; inset graph: non-linear fit for i_{lim} and v

action at the S-MBEAs of BDD to be controlled by linear diffusion-limited transport. Several researchers[15,20] reported that different diffusion layers of MEA would overlap if the interelement spacing of MEA was not large enough. As a result, the entire geometrical area would behave like a macroelectrode to form linear diffusion-limited transport at MEA surface. In our work, the ratio of the interelement spacing of the microbands to the width of microband (d/w) is 5 which could not entirely avoid the overlap of diffusion layers along the adjacent microband electrodes. So the CV curves exhibit a typically linear diffusion-limited transport for the $K_4Fe(CN)_6/K_3Fe(CN)_6$ redox system. In addition, the peak-to-peak separation (ΔE_p) of S_1-MBEA and S_2-MBEA of BDD is greater than 80 mV, indicating a quasi-reversible process in the ferri–ferrocyanide redox system. Furthermore, the shapes of CV curves at S_1-MBEA and S_2-MBEA are similar, which indicates that the electrochemical characters of two S-MBEAs in our work are similar. In other words, the I-MBEA electrode prepared in our work is symmetrical and can be used random group of parallel microbands to measure electrochemical characteristics.

As shown in Fig. 3c, the shapes of CV curves of I-MBEA at BDD surface are different from those of S-MBEAs tending towards sigmoidal shapes. A quasi-steady current limit is reached. It clearly shows that the current limit is not proportional to $v^{1/2}$ but increases a little with increasing v and then

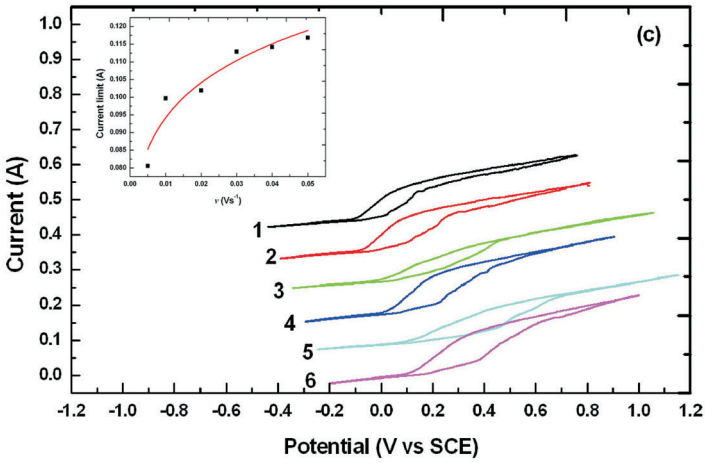

FIG. 3
(*Continued*)

approaches a quasi-steady-state non-linear diffusion of I-MBEA of BDD in the ferri–ferrocyanide redox system.

Soh et al.[20,24,25] proposed that mass transport to the element for MEA was enhanced for the small sizes of MEA. The diffusion layer of every microelectrode would not overlap but exhibit the edge effect if the interelement spacing of MEA was large enough. Thus, CV curves would show hemispherical steady-state diffusion profile to form a sigmoidal shape aided by the intense edge effect. The current limit was independent of *v*, i.e. it kept the same value with increasing *v*. The element diffusion in our work is between linear and hemispherical diffusion of the I-MBEA at BDD surface. This could be explained by the structure of I-MBEA (see Fig. 1). I-MBEA consist of two groups of interdigitated parallel microbands, one group as S_1-MBEA and another group as S_2-MBEA. The microbands of two S-MBEAs are located partly face-to-face which is called as interdigitated part. Another part of microbands not in face-to-face section is called paralleling part. The length of interdigitated part microbands is 50 μm and that of paralleling-part microbands is 10 μm. Then, the element diffusion of I-MBEA at the BDD surface can be predicted as follows. The diffusion of interdigitated part of microband electrode is screened to avoid the overlap of diffusion layer showing the edge effect to partly obtain the hemispherical diffusion. On the other hand, the diffusion of the paralleling part exhibits linear diffusion for the overlap of diffusion layer. So the element diffusion at I-MBEA is combined with linear and hemispherical diffusion. The Seddon research group[26] defined the current limit of hemispherical diffusion in microband electrode, i_l, as

$$i_l = \frac{2\pi m n D F c l}{\ln(4\pi^2 D t / w^2)} \tag{3}$$

with $t = RT/Fv$, where *m* is the number of individual elements, *n* is the number of electrons taking part in electron transfer reaction, *D* is the diffusion coefficient of the analyte, *F* is Faraday constant, *c* is the concentration of the analyte, *l* and *w* are the length and width of the microband element, respectively, *R* is the gas constant, *T* is the reaction temperature and *v* is the sweep rate. Then we assume in this work that the current limit, i_{lim}, is a function of *v*, as the combination of current limit from hemispherical diffusion (i_l), peak current from linear diffusion (i_p) and other influence factors from electric inductance behavior of the I-MBEA at BDD surface. So, i_{lim} can be expressed as

$$i_{lim} = b_1 i_l + b_2 i_p + b_3 v^{b_4} + b_5 \quad (4)$$

where b_1 and b_2 are self-defined constants related to the contribution of hemispherical and linear diffusion, respectively, i_p can be obtained as a function of v from the linear fit results of the peak current and $v^{1/2}$ for S_1-MBEA and S_2-MBEA. Here the linear-fit expression was used for S_2-MBEA. The other self-defined constants, b_3 and b_4, are related to contribution of electric inductance behavior of the I-MBEA at BDD surface, b_5 is a constant factor.

Thus, we used the non-linear fitting function of Origin 6.0 software to obtain the values of these constants by allowing for literature values of the diffusion coefficient, $D = 7.35 \times 10^{-6}$ cm^2 s^{-1} (ref.[27]), and one electron being involved in the electron transfer process at 298 K. The fitting results of Eq. (*4*) with Chi square value of fitting lower than 2.0×10^{-5} (correlation coefficient greater than 0.93) are listed in Table I and the fitting graph was shown as the inset graph of Fig. 3c.

TABLE I
Fitting result of non-linear fitting function for current limit i_{lim} and v

b_1	b_2	b_3	b_4	b_5	Chi square of fitting	Correlation coefficient
1.10	0.87	0.18	0.14	2.95×10^{-2}	2.0×10^{-5}	0.93

Apparently, the constant, b_1, is higher than b_2 which suggests the hemispherical diffusion is primary for the I-MBEA at BDD surface. The current limit for I-MBEA is about 1000 times higher than the peak current for S-MBEAs, which can be interpreted that the measurement limit would improve greatly for I-MBEA in electrochemical analysis system.

Impedance Properties of S-MBEA and I-MBEA at BDD Surface

Electrochemical impedance spectra (EIS) analysis is a useful technique to investgate the reaction process and the charge transfer characteristic at electrode surfaces. Figure 4 displays impedance Nyquist plots of S_1-MBEA and S_2-MBEA obtained at the open-circuit potential in 0.1 M $K_4Fe(CN)_6$ and 0.4 M KNO_3 solution. Based on the shape of Nyquist graphs with two curvatures, there are two time constants in the redox system. It predicts that

there are two state variables in the surface reaction of the electrode process. A similar result was obtained at the planar BDD electrode surface by the other researchers[28,29]. By adopting the electrical equivalent circuit model with two time constants (Fig. 5) and using ZsimpWin software to simulate the experimental data, the fitting values of the electric elements are calculated and listed in Table I with the variance lower than 1.09×10^{-3} and 1.16×10^{-3}, respectively.

The electric elements of equivalent circuit for the S-MBEAs include solution resistance (R_s), additional polarization resistance (R_t), double layer capacitance (C_{dl}), impedance corresponding to the space charge of diamond (CPE), space charge resistance of diamond ($R_{diamond}$) and Warburg imped-

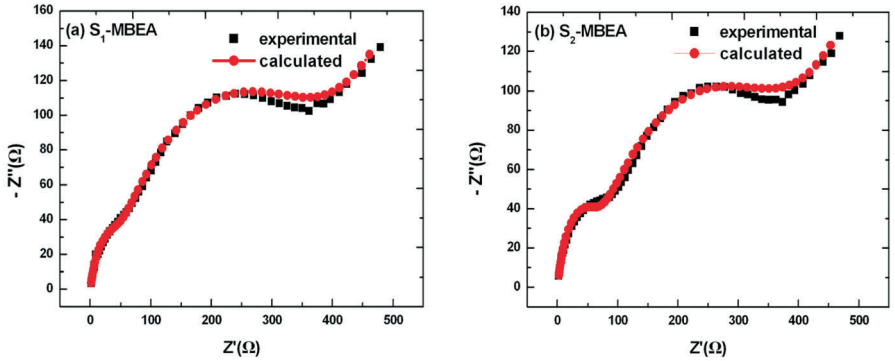

FIG. 4

Impedance Nyquist plots at: a S_1-MBEA and b S_2-MBEA. Measured for 0.1 M $K_4Fe(CN)_6$ and 0.4 M KNO_3 solution; ■ experimental data, –●– calculated from the electrical equivalent circuit model fitting

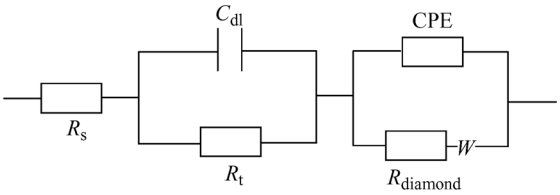

FIG. 5

Graph of electrical equivalent circuit model of S_1-BEMA and S_2-BEMA. R_s, solution resistance; R_t, additional polarization resistance; C_{dl}, double layer capacitance; CPE, impedance corresponding to the space charge of diamond; $R_{diamond}$, space charge resistance of diamond; W, Warburg impedance

ance (W). The values of R_s at S_1-MBEA and S_2-MBEA are similar in the electrochemical systems for R_s lies on the solution characteristic (Table II). Apparently, the value of $R_{diamond}$ is larger than that of R_s or R_t which can be explained by the moderately boron-doped level of BDD electrode in our work. Furthermore, $R_{diamond}$ and W for the two S-MBEAs are nearly equal. The values of these electrical elements are confirmed by the characteristic of polycrystalline surface of diamond including the crystal size, boron contents and adsorbed group. All of the diamond characteristics for S_1-MBEA and S_2-MBEA are similar for the BDD film is same and uniform. Similar electrochemical characteristics are also obtained by CV analysis (see Figs 3a

TABLE II
Values of the electrical elements calculated from equivalent circuit model of S_1-MBEA and S_2-MBEA

	R_s Ω	R_t Ω	C_{dl} F cm^{-2}	CPE S–s^n cm^{-2}	n	$R_{diamond}$ Ω	W Ω	Variance
S_1-MBEA	10^{-7}	28.95	1.37×10^{-6}	8.47×10^{-5}	0.62	387.2	2.47×10^{-3}	1.09×10^{-3}
S_2-MBEA	10^{-7}	48.01	5.66×10^{-7}	1.11×10^{-5}	0.58	377.7	2.77×10^{-3}	1.16×10^{-3}

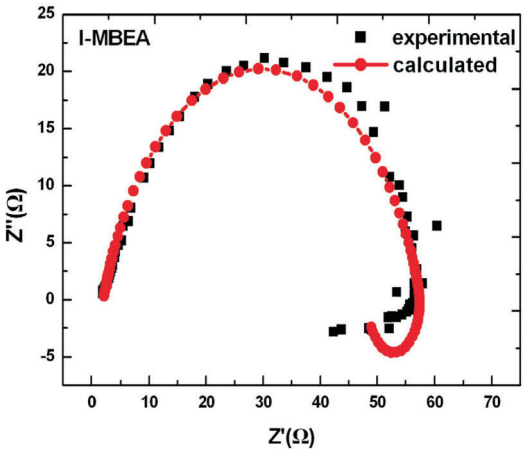

FIG. 6
Impedance Nyquist plots of I-MBEA on BDD electrodes measured for 0.1 M $K_4Fe(CN)_6$ and 0.4 M KNO_3 solution; ■ experimental data, –●– calculated from the electrical equivalent circuit model fitting

and 3b). The other electric elements are different because the inevitable errors from microfabrication process of MBEA induce a small difference between physical parameters of S_1-MBEA and S_2-MBEA, such as the active area of electrodes.

Figure 6 shows impedance Nyquist plots obtained at an open-circuit potential in 0.1 M $K_4Fe(CN)_6$ and 0.4 M KNO_3 solution at the I-MBEA surface. Based on the shape with only one curvature, it is clear that there is only one time constant in the redox system displaying the surface reaction of the electrode process with one state variable. In addition, there is a large semicircle at low frequencies accompanied by a small curvature in the forth quadrant. The negative peak also is observed in phase shift plot due to inductive behavior[30]. By adopting the electric equivalent circuit model (Fig. 7) and using ZsimpWin software to simulate the experimental data, the fitting values of electric elements with variance lower than 4.84×10^{-3} are listed in Table III.

The electric elements of equivalent circuit for the I-MBEA include solution resistance (R_s), additional polarization resistance (R_t), impedance corresponding to the space charge of diamond (CPE), space charge resistance of

TABLE III
Values of the electrical elements calculated from equivalent circuit model of I-MBEA

	R_s Ω	R_t Ω	CPE S–s^n cm^{-2}	n	$R_{diamond}$ Ω	L H	Variance
I-MBEA	2.04	55.62	6.80×10^{-5}	0.80	274.2	1261	4.84×10^{-3}

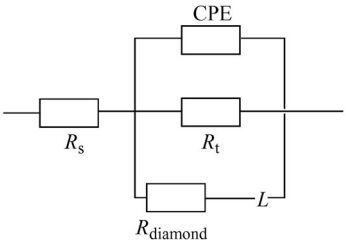

FIG. 7
Graph of electrical equivalent circuit model of I-BEMA. R_s, solution resistance; R_t, additional polarization resistance; CPE, impedance corresponding to the space charge of diamond; $R_{diamond}$, space charge resistance of diamond; L, electronic inductance of diamond

diamond ($R_{diamond}$) and electronic inductance of diamond (L). Compared with those of the S-MBEAs, there is an equivalent electronic inductance, L, of an I-MBEA at BDD surface. Some researchers[30,31] proposed that the inductive behavior occured for relaxation phenomenon characteristics of the generation of further active sites and further adsorption of electroactive constituents on active sites. Additionally, there were some active substances produced at the BDD electrode surface, such as active hydroxy groups to enhance inductance response. Furthermore, the inductance effect could be presented by a negative differential capacitance and a negative differential resistance in the electric equivalent circuit model. So, by adopting the electric equivalent circuit model (Fig. 8), the fitting values of electric elements with variance lower than 4.74×10^{-3} are listed in Table IV.

TABLE IV
Values of the electrical elements calculated from equivalent circuit model without electronic inductance element of I-MBEA

	R_s Ω	R_t Ω	CPE S–s^n cm^{-2}	n	R_d Ω	C_d F cm^{-2}	Variance
I-MBEA	1.54×10^{-2}	0.42	9.01×10^{-3}	0.80	-7.04×10^{-2}	–56.4	4.74×10^{-3}

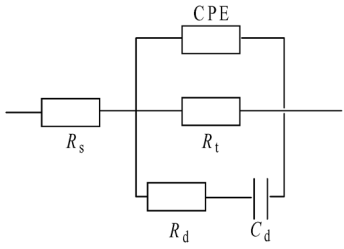

FIG. 8
Graph of electrical equivalent circuit model without electronic inductance element of I-BEMA. R_s, solution resistance; R_t, additional polarization resistance; CPE, impedance corresponding to the space charge of diamond; R_d, negative differential resistance of diamond, C_d, negative differential capacitance of diamond

CONCLUSION

Electrochemical properties of single microband electrode arrays (S-MBEA) and interdigitated microband electrodes arrays (I-MBEA) of BDD film are strongly different in CV analysis. The $Fe(CN)_6^{3-/4-}$ redox reaction in S-MBEAs is controlled by linear diffusion-limited transport because the ratio d/w is small and could not avoid the overlap of diffusion layer along the adjacent microband electrodes. But the redox process in I-MBEA approaches a quasi-steady-state non-linear diffusion because of the intense edge effect of every microband of BDD electrode film. The relation between current limit, i_{lim}, and v was obtained (correlation coefficient greater than 0.93) by defining i_{lim} as a combination of current limit from hemispherical diffusion, peak current from linear diffusion and the influence factors from electric inductance behavior of the I-MBEA at BDD surface. Comparing the values of constants, the hemispherical diffusion is primary in the I-MBEA at BDD surface. The current limit in I-MBEA is about 1000 times higher than the peak current in S-MBEAs.

The charge transfer characteristics of S-MBEA and I-MBEA at BDD surface have been studied by EIS analysis. There are two time constants in S-MBEA and only one time constant in I-MBEA surface in the redox system.

By arranging the microbands as interdigitated form, MBEA can display the characteristic of MEA independently of whether the interelement spacing is larger enough or not. So, I-MBEA is an interesting MEA form to measure some metal ions, organic compounds and other pollutants in electrochemical microanalysis using a smaller electrode area and sample volume.

REFERENCES

1. Harrison T. S.: *J. Hist. Neurosci.* **2000**, *9*, 165.
2. Reller H., Kirowa-Eisner E., Gileadi E.: *J. Electroanal. Chem. Interfacial Electrochem.* **1984**, *161*, 247.
3. Cassidy J., Ghoroghchian J., Sarfarazi F., Smith J. J., Pons S.: *Electrochim. Acta* **1986**, *31*, 629.
4. Strojek J. W., Granger M. C., Dallas T., Holtz M. V., Swain G. M.: *Anal. Chem.* **1996**, *68*, 2031.
5. Lee J., Einaga Y., Fujishima A., Park S.-M.: *J. Electrochem. Soc.* **2004**, *151*, E265.
6. Perret A., Haenni W., Skinner N., Tang X.-M., Gandini D., Comninellis C., Correa B., Foti G.: *Diamond Relat. Mater.* **1999**, *8*, 820.
7. Dragoe D., Spătaru N., Kawasaki R., Manivannan A., Spătaru T., Tryk D. A., Fujishima A.: *Electrochim. Acta* **2006**, *51*, 2437.
8. Manivannan A., Ramakrishnan L., Seehra M. S., Granite E., Butler J. E., Tryk D. A., Fujishima A.: *J. Electroanal. Chem.* **2005**, *577*, 287.

9. Fujishima A., Rao T. N., Popa E., Sarada B. V., Yagi I., Tryk D. A.: *J. Electroanal. Chem.* **1999**, *473*, 179.
10. Pedrosa V. A., Codognoto L., Machado S. A. S., Avaca L. A.: *J. Electroanal. Chem.* **2004**, *573*, 11.
11. Ivandini T. A., Sarada B. V., Terashima C., Rao T. N., Tryk D. A., Ishiguro H., Kubota Y., Fujishima A.: *J. Electroanal. Chem.* **2002**, *521*, 117.
12. Preechaworapun A., Chuanuwatanakul S., Einaga Y., Grudpan K., Motomizu S., Chailapakul O.: *Talanta* **2006**, *68*, 1726.
13. Bouvrette P., Hrapovic S., Male K. B., Luong J. H. T.: *J. Chromatogr., A* **2006**, *1103*, 248.
14. Davies T. J., Compton R. G.: *J. Electroanal. Chem.* **2005**, *585*, 63.
15. Hye Jin Lee, Beriet C., Ferrigno R., Girault H. H.: *J. Electroanal. Chem.* **2001**, *502*, 138.
16. Provent C., Haenni W., Santoli E., Rychen P.: *Electrochim. Acta* **2004**, *49*, 3737.
17. Kapałka A., Fóti G., Comninellis C.: *Electrochem. Commun.* **2008**, *10*, 607.
18. Bjorefors F., Strandman C., Nyholm L.: *Electroanalysis* **2000**, *12*, 255.
19. Soh K. L., Kang W. P., Davidson J. L., Basu S., Wong Y. M., Cliffel D. E., Bonds A. B., Swain G. M.: *Diamond Relat. Mater.* **2004**, *13* 2009.
20. Soh K. L., Kang W. P., Davidson J. L., Wong Y. M., Cliffel D. E., Swain G. M.: *Diamond Relat. Mater.* **2008**, *17*, 240.
21. Katsuyoshi H., Yuzuru I., Ryoji K., Kenji S., Osamu N., Akiyuki T.: *J. Electroanal. Chem.* **2005**, *579*, 215.
22. Katsuyoshi H., Yuzuru I., Ryoji K., Kenji S., Osamu N.: *Electrochem. Commun.* **2003**, *5*, 1037.
23. Wei J. J., He Q., Gao X. H.: *J. Synth. Cryst.* **2007**, *36*, 569.
24. Cheng C. X., Jü Y. X., Chen H. Z.: *Chem. J. Chinese Univ.* **1995**, *16*, 854.
25. Morf W. E., Koudelka-Hep M., de Rooij N. F.: *J. Electroanal. Chem.* **2006**, *590*, 47.
26. Sheddon B. J., Eddowes M. J., Firth A., Owen A. E., Girault H. H. J.: *Electrochim. Acta* **1991**, *36*, 763.
27. Southampton Electrochemistry Group: *Instrumental Methods in Electrochemistry* (in Chinese), p. 191. Fudan University Press, Shanghai 1992.
28. Liu F. B., Li X. M., Wang J. D., Liu B., Chen D. R.: *Chin. Sci. Bull.* **2006**, *51*, 1344.
29. Ramesham R.: *Thin Solid Films* **1998**, *315*, 222.
30. Danaeea I., Jafariana M., Forouzandeha F., Gobalb F., Mahjania M. G.: *Electrochim. Acta* **2008**, *53*, 6602.
31. Seland F., Tunold R., Harrington D. A.: *Electrochim. Acta* **2006**, *51*, 3827.